commercially available sizes to obtain minimum weight. Obviously, this is a function of the specific application.

References

[1] Shanley, F., *Weight Strength Analysis of Aircraft Structures*, 1st ed., McGraw-Hill, New York, 1952; 2nd ed., Dover, New York, 1960.

[2] Vinson, J. R. and Shore, S., "Bibliography on Methods of Structural Optimization for Flat Sandwich Panels," NAEC-ASL-1082, April 1965, Naval Air Engineering Center, Philadelphia, Pa.

[3] Vinson, J. R. and Shore, S., "Methods of Structural Optimization for Flat Sandwich Panels," NAEC-ASL-1083, April 1965, Naval Air Engineering Center, Philadelphia, Pa.

[4] Vinson, J. R. and Shore, S., "Design Procedures for the Structural Optimization of Flat Sandwich Panels," NAEC-ASL-1084, April 1965, Naval Air Engineering Center, Philadelphia, Pa.

[5] Vinson, J. R. and Shore, S., "Structural Optimization of Corrugated Core and Web Core Sandwich Panels Subjected to Uniaxial Compression," NAEC-ASL-1109, May 1967, Naval Air Engineering Center, Philadelphia, Pa.

[6] Vinson, J. R. and Shore, S., "Minimum Weight Corrugated Core Sandwich Panels Subjected to Uniaxial Compression," *Fibre Science and Technology*, Vol. 1, No. 2, Oct. 1968, pp. 151–163.

[7] Vinson, J. R. and Shore, S., "Structural Optimization of Flat Corrugated Core Sandwich Panels Under In-Plane Shear Loads and Combined Uniaxial Compression and In-Plane Shear Loads," NAEC-ASL-1110, July 1967, Naval Air Engineering Center, Philadelphia, Pa.

[8] McCoy, T. T., Shore, S., and Vinson, J. R., "A Method for Weight Optimization of Flat Truss Core Sandwich Panels Under Lateral Loads," NAEC-ASL-1111, July 1967, Naval Air Engineering Center, Philadelphia, Pa.

[9] Libove, C., and Hubka, R. E., "Elastic Constants for Corrugated Core Sandwich Plates," TN 2289, Feb. 1951, NACA.

[10] Seide, P., "The Stability Under Longitudinal Compression of Flat Symmetric Corrugated-Core Sandwich Plates With Simply Supported Loaded Edges and Simply Supported or Clamped Unloaded Edges;" TN 2679, April 1952, NACA.

[11] "Structural Sandwich Composites," MIL-HDBK-23, April 1967, Dept. of Defense, Washington, D.C.

[12] Timoshenko, S. and Gere, J., *Theory of Elastic Stability*, 2nd ed., McGraw-Hill, New York, 1961, p. 404.

[13] Schmit, Jr., L. A., Morrow, W. M., II, and Kicher, T. P., "A Structural Synthesis Capability for Integrally Stiffened Cylindrical Shells," AIAA Paper 68-327, 1968, New York.

[14] "Strength of Metal Aircraft Elements," MIL-HDBK-5, March 1959, Armed Forces Supply Support Center, Washington, D.C. (newer addition is "Metallic Materials and Elements For Flight Vehicle Structures," MIL-HDBK-5A, Feb. 1966, U.S. Government Printing Office, Washington, D.C.).

[15] Letter from K. H. Boller, Forest Products Lab., to R. T. Molella, Naval Air Engineering Center, Philadelphia, Pa., September 30, 1964: Code 4000 (A.S.D.).

[16] "Plastic for Flight Vehicles, Part 1, Reinforced Plastics," MIL-HDBK-17, Change Notice 1, May 1964, Armed Forces Supply Support Center, Washington, D.C.

[17] "Beryllium in Aerospace Structures," Brush Beryllium Co., Cleveland, Ohio.

NOVEMBER 1971 J. AIRCRAFT VOL. 8, NO. 11

Jet Noise Excitation of an Integrally Stiffened Panel

MERVYN D. OLSON*
University of British Columbia, Vancouver, Canada
AND
GARRY M. LINDBERG†
National Aeronautical Establishment, National Research Council, Ottawa, Canada

The free vibrations and random response to jet noise of an integrally stiffened five bay panel have been studied both theoretically and experimentally. A finite element approach was used to represent the panel for both parts of the study, and the predictions were verified by measurements on a model panel integrally machined from solid Aluminum stock. The comparison between predicted and measured vibration modes and frequencies revealed good correlation of frequencies while the correlation of mode shapes was only fair, especially for higher modes. The predicted modes and frequencies were used in a modal analysis of the panel's response to jet noise with a consistent finite element method being introduced to calculate the required cross spectral modal force terms. Quantitative agreement between predicted and measured rms stresses and displacements was realized, whereas only qualitative agreement was obtained for the associated spectra.

Nomenclature

a_l, b_l, c_l = finite-element dimensions, Fig. 9
c_o = speed of sound
$e_i, \{E\}$ = polynomial coefficients, Eq. (9)
$f_j(x,y)$ = jth mode shape
$\{F(\xi,\eta)\}$ = column vector of polynomial terms, Eq. (7)
$H_j(\omega)$ = complex admittance for jth mode
$I_{jk}(\omega)$ = modal force cross spectral matrix, Eq. (4)
m_j = generalized mass for jth mode
p_o = root mean square pressure
$\{P_0\}, \{P_1\}, \{P_2\}$ = consistent finite-element load vectors
$[Q(\omega)]$ = cross spectral matrix for generalized coordinates, Eq. (17)
$R(\bar{x},\bar{y},\tau)$ = noise correlation function, Eq. (2)
w = panel and finite-element displacement
w_{rms} = root mean square displacement
$\{W\}$ = column vector of generalized displacements for finite element, Eq. (8)
ζ_j = damping ratio for jth mode

Received November 23, 1970; presented as Paper 71-585 at the AIAA 4th Fluid and Plasma Dynamics Conference, Palo Alto, Calif., June 21-23, 1971; revision received July 21, 1971. Work carried out at the National Aeronautical Establishment.

Index categories: Aircraft Vibration; Structural Dynamic Analysis.

* Assistant Professor, Dept. of Civil Engineering. Member AIAA.

† Associate Research Officer, Structures and Materials Laboratory. Member AIAA.

σ_{rms} = root mean square stress
$\phi_{pp}(\bar{x},\bar{y},\omega)$ = noise cross spectral density function, Eq. (3)
$\phi_{ww}(x_1,\dots)$ = response cross spectral density function, Eq. (5)
ω = circular frequency
ω_j = natural frequency of jth mode
$(\ )^*$ = complex conjugate of $(\ )$

Introduction

THE response of aerospace structures to random pressure fields as, for example, encountered in turbulent boundary layers and adjacent to jet exhausts has been the subject of considerable research work. (See Refs. 1–3 for extensive bibliographies). Much of this work has concerned simple panels, built-up rib stringer systems and more recently integrally stiffened panels. The theoretical studies break naturally into two parts, namely, free vibration predictions and random response predictions for the structure. To predict the frequencies and modes of complex multibay panel systems, several approximate techniques have been developed, the most notable ones being the transfer matrix method[4–6] and the finite element method.[7–9] The random response of such structures has been calculated using the modal approach[10–14] and more recently by a direct finite element method.[7,9,15]

On the experimental side, good quantitative response data has only been available for relatively simple panels. Although many tests on built-up stiffened panels have been carried out, most of these have been for proof testing against fatigue or for developing design chart criteria[16] and are therefore largely unsuitable for verifying theoretical response predictions. Response data for integrally stiffened panels is virtually nonexistent (Ref. 6 is an exception).

In the present work, the dynamics of just such an integrally stiffened panel were studied both theoretically and experimentally. The purposes of the study were to verify the application of the now well-known finite element method to such structural configurations, and secondly, to gain an understanding of the random response of integrally stiffened plates. The particular configuration of a five-bay panel with length to width ratio of 5 to 2 was taken as a typical stiffened structure (Fig. 1). New refined triangular plate bending elements[17,18] and refined beam bending and torsional elements were employed in the panel analysis.

The free vibrations of the panel were predicted with the foregoing finite elements, and these predictions were then verified experimentally. The response of the panel to jet noise excitation was then considered. Theoretical calculations based on the well-known modal method[10,11] were carried out. However, the approach used was novel in that the mode shapes and frequencies predicted by the finite elements were used, and a consistent finite element method for calculating the modal force cross spectra matrix was developed. A model cross spectral density function for the pressure excitation on the panel was obtained from correlation measurements in the jet noise field, and this model was used as input for the above calculations. Finally, an experimental investigation of the panel response in a freejet noise field was carried out to verify the predictions. A preliminary and somewhat brief presentation of the following work was given in Ref. 19, and the full details are available in Ref. 20.

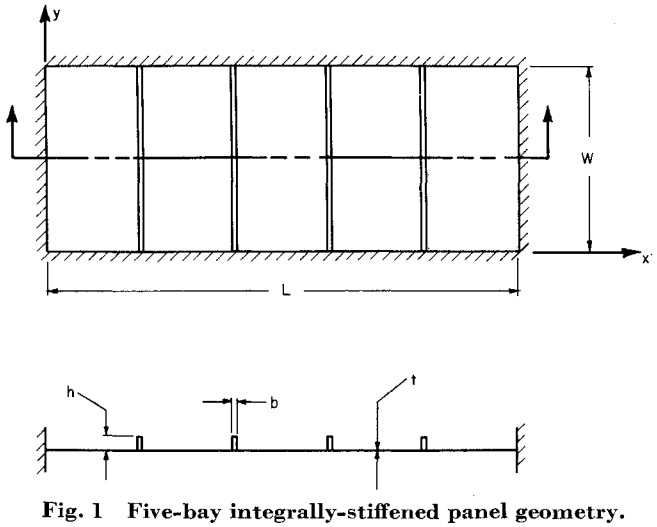

Fig. 1 Five-bay integrally-stiffened panel geometry.

Free Vibrations

Using the double symmetry available, only one quarter of the panel was analyzed with the finite element gridwork shown in Fig. 2. As shown, two nodes were used adjacent to the stringers and the following special constraints were introduced between the degrees of freedom at these nodes

$$w_R = w_L + b(\partial w/\partial x)_L,\ (\partial w/\partial y)_R = (\partial w/\partial y)_L + b(\partial^2 w/\partial x \partial y)_L \quad (1a,b)$$

$$(\partial^2 w/\partial y^2)_R = (\partial^2 w/\partial y^2)_L,\ (\partial w/\partial x)_R = (\partial w/\partial x)_L \quad (1c,d)$$

$$(\partial^2 w/\partial x \partial y)_R = (\partial^2 w/\partial x \partial y)_L \quad (1e)$$

where subscripts R, L mean right, left. Note that curvatures $\partial^2 w/\partial x^2$ were not constrained and hence, could take up different values on either side of the stiffeners. The beam bending and torsion degrees of freedom were equated to averages of the corresponding plate degrees of freedom, i.e., $w_B = (w_L + w_R)/2$, etc. After applying clamped boundary, symmetry and constraint conditions, each subproblem had the following net degrees of freedom: 1) symmetric in x and y, 58, 2) antisymmetric in x and symmetric in y, 53, 3) symmetric in x and antisymmetric in y, 45 and 4) antisymmetric in x and y, 42. Some of the predicted frequencies are given in Table 1, and corresponding mode shapes are shown in Figs. 3(a–c). The numbers in the symmetry columns of Table 1 refer to the number of half waves per bay in x and y.

The experimental panel model was integrally machined from a 1 in. thick sheet of aluminum, and the measurements were made by standard resonance testing. The panel was excited with several (1–4) acoustic drivers which could be driven either in or out of phase with each other. The response was measured with strain gauges and inductance probes, and the nodal patterns of Fig. 3 were obtained with sugar crystals.

It is seen that the modes separate into definite groups containing either five or four modes. The groups of five correspond to panel modes, whereas the groups of four correspond to stiffener modes. Within each group, the mode shapes generally exhibit the same amount of waviness in either direction, but have different phase changes from peak to peak. Only one stiffener mode group is shown here, but higher ones involving torsion as well were obtained. The agreement between the predicted and measured frequencies was generally

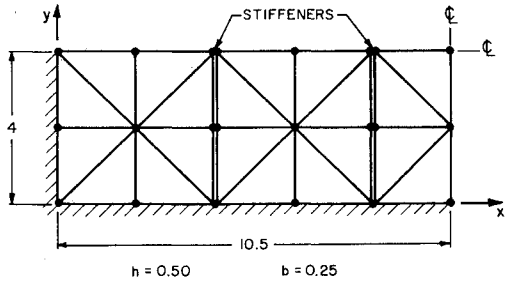

Fig. 2 Finite element grid for detailed calculation of vibration modes and frequencies.

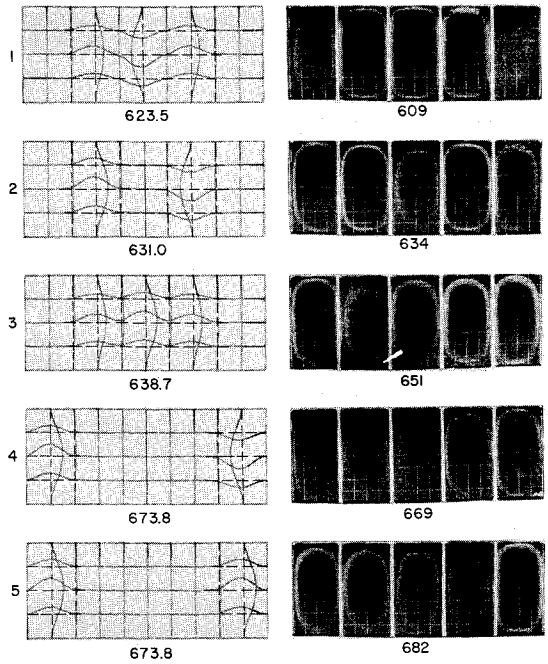

Fig. 3a Experimental and theoretical modes 1 to 5.

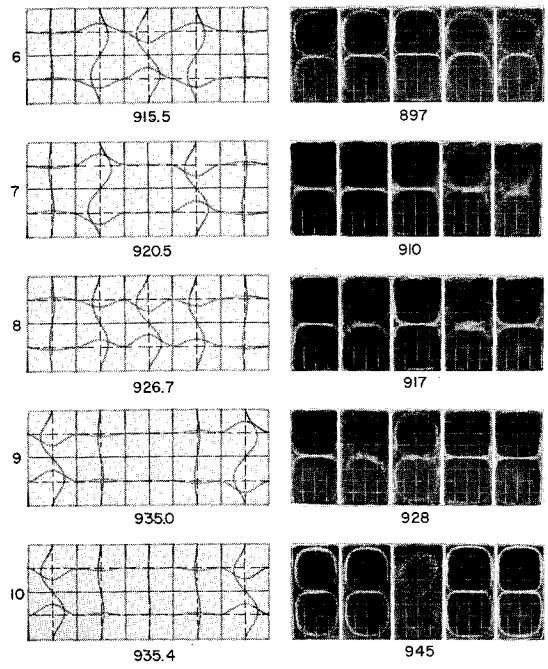

Fig. 3b Theoretical and experimental modes 6 to 10.

very good (the comparison is extended to a total of eighty modes in Ref. 20), whereas some differences in mode shapes were observed. The main differences were between relative amplitudes from bay to bay. The measured amplitudes were generally distributed more evenly across the panel than were the predicted ones, especially for higher modes. This effect seems to be a result of slight imperfections in the model and hence is very difficult to remove.

The apparent damping in the panel was estimated by measuring half-power widths at modal resonances and/or by measuring the logarithmic decrement on decaying modal response traces. The results in terms of ratios of damping present to critical damping or ζ for particular modes are shown in Fig. 4. These measurements were extremely difficult to carry out and considerable scatter was obtained even for repeatable modes. The main reason for the difficulty was the obvious near proximity of the panel modes. This proximity resulted in response overlap away from the peaks, which obscured the half-power measurements, and led to beating in the decay traces. Consequently, it was felt that the results of Fig. 4 were sufficiently reliable only to provide an average value to be used in the response calculations. This average was taken to be 0.002, as shown.

On the other hand, these damping results were good enough to show that for this type of stiffened panel, the damping is not a simple function of frequency. On the contrary, it seems to be a complicated function of mode shape as well. For example, the damping ratios for modes 1–5 varied from 0.001 to 0.003. Some of this large variation is probably due to the acoustic coupling with the surrounding air, which is highly dependent on mode shape. This question of panel damping requires further research.

Response to Jet Noise

The response of the foregoing stiffened panel subjected to jet noise excitation is described here. Figure 5 shows the experimental setup which consisted of a fairly rigid baffle positioned adjacent to but outside of the jet efflux. Correlation measurements in the noise field on the baffle were made using two Bruel and Kjaer $\frac{1}{4}$ in. microphones with a rigid insert in place of the panel. These measurements were then fitted with the simple exponentially decaying plane wave propagating model:

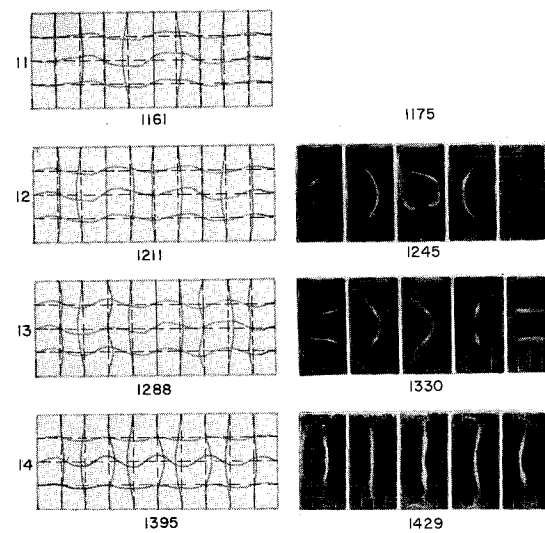

Fig. 3c Theoretical and experimental modes 11 to 14.

$$R(\bar{x},\bar{y},\tau) = \exp[-\alpha_1|\tau - \bar{x}/c_o| - \alpha_2|\bar{x}| - \alpha_3|\bar{y}|]\cos\omega_0(\tau - \bar{x}/c_o) \quad (2)$$

The fit of this model to the data at various positions in the streamwise direction is shown in Fig. 6. The numerical results for this fit were $\alpha_1 = 4500$/sec, $\alpha_2 = 0.050$/in., $\alpha_3 = 0.037$/in., $\omega_0 = 8000$ rad/sec and $c_0 = 14{,}000$ in./sec (speed of sound). Equation (2) is Fourier transformed to yield the cross spectral density function for the noise excitation as

$$\phi_{pp}(\bar{x},\bar{y},\omega) = p_o^2 \frac{\alpha_1/\pi[\alpha_1^2 + \omega_0^2 + \omega^2]}{[\alpha_1^2 + (\omega - \omega_0)^2][\alpha_1^2 + (\omega + \omega_0)^2]} \times \exp[-\alpha_2|\bar{x}| - \alpha_3|\bar{y}| - i\omega\bar{x}/c_o] \quad (3)$$

where p_o^2 is the mean square pressure, which was assumed to be constant over the panel area. The power spectral density from this model, $\phi_{pp}(0,0,\omega)$ is compared in Fig. 7 with experimental results obtained by both a direct and an indirect method. In the direct method, a General Radio Wave

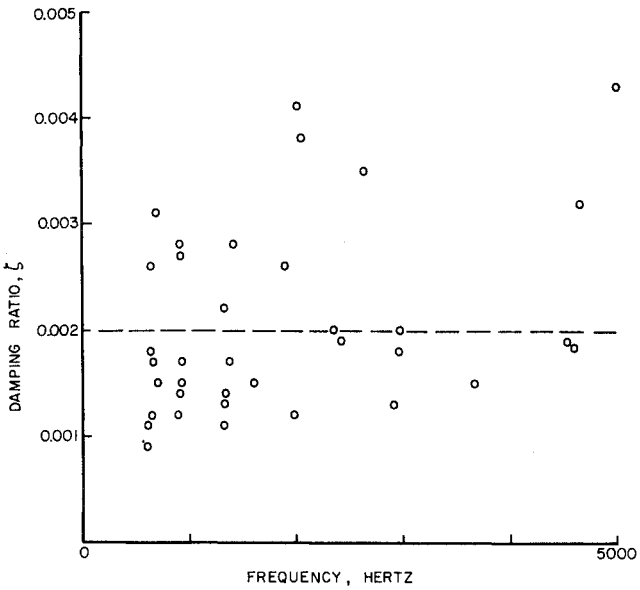

Fig. 4 Damping ratio for five-bay panel.

Analyzer Model 1900A and Graphic Level Recorder Model 1521B were employed with a bandwidth of 50 Hz, writing speed of 3 in./sec, and traverse speed of 208 Hz/min. The indirect results are from a numerical Fourier transform of the noise autocorrelation measurements using 300 lag points from 0 to 15 msec. The two results compare quite well, although it appears that the model is too high by a factor of two around 600 Hz.

Following Lin,[11] the cross spectral density of the generalized forces for the free vibration modes j and k is

$$I_{jk}(\omega) = \iiiint \phi_{pp}(\bar{x},\bar{y},\omega) f_j(x_1,y_1) f_k(x_2,y_2) dx_1/dy_1 dx_2 dy_2 \quad (4)$$

where $\bar{x} = x_2 - x_1$, $\bar{y} = y_2 - y_1$, $f_j(x,y)$ is the jth mode, and the two integrations are each over the whole panel. Once the I_{jk} are known, the cross spectral density of the responses at

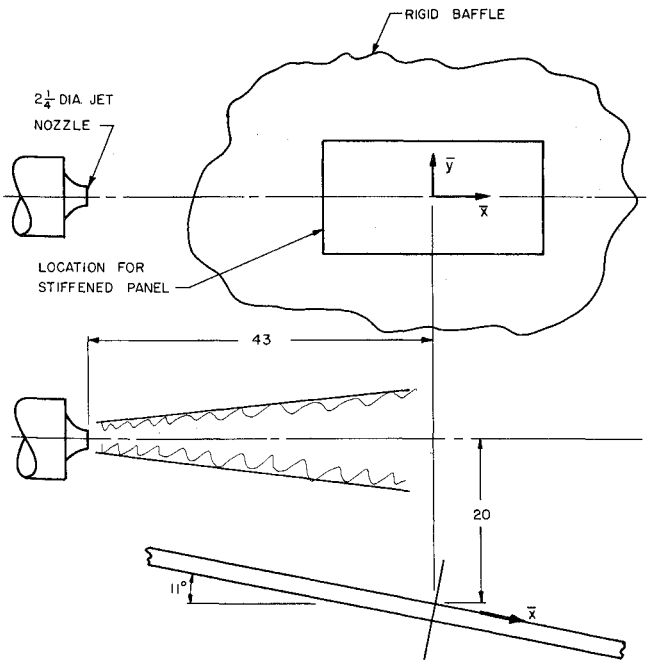

Fig. 5 Experimental setup for jet noise and response measurements.

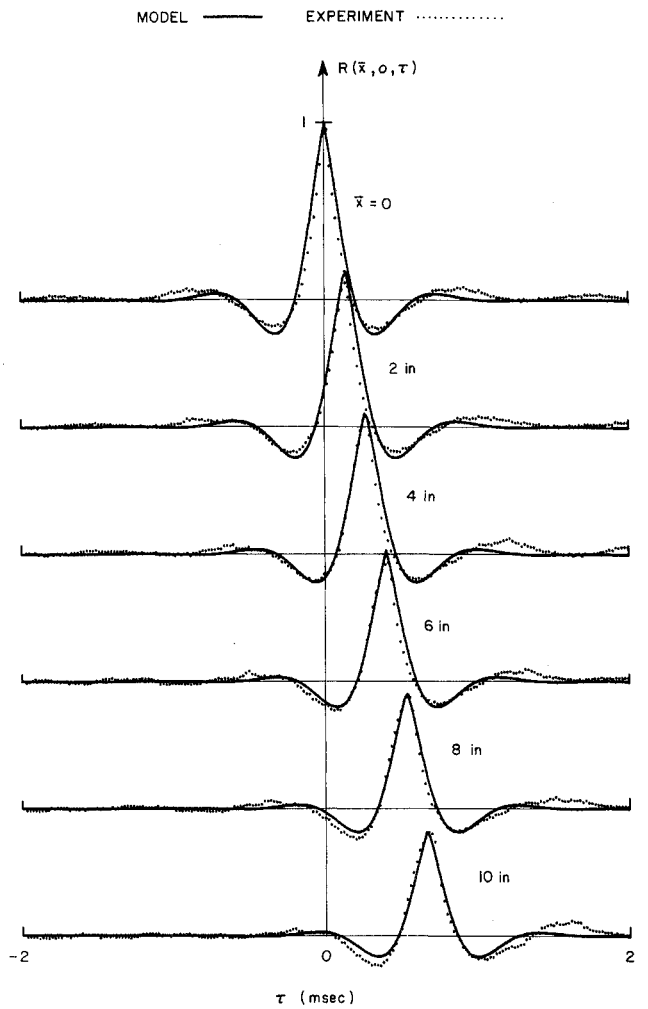

Fig. 6 Comparison of model and experimental correlation functions.

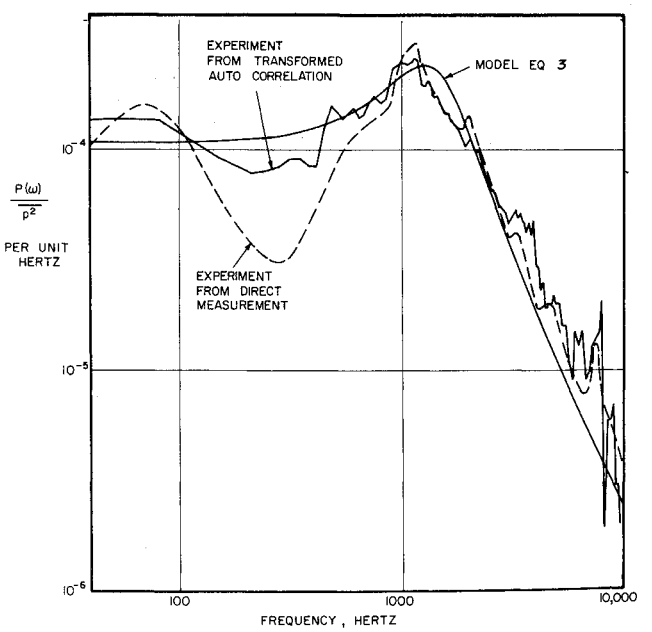

Fig. 7 Comparison of model and measured power spectral density of noise.

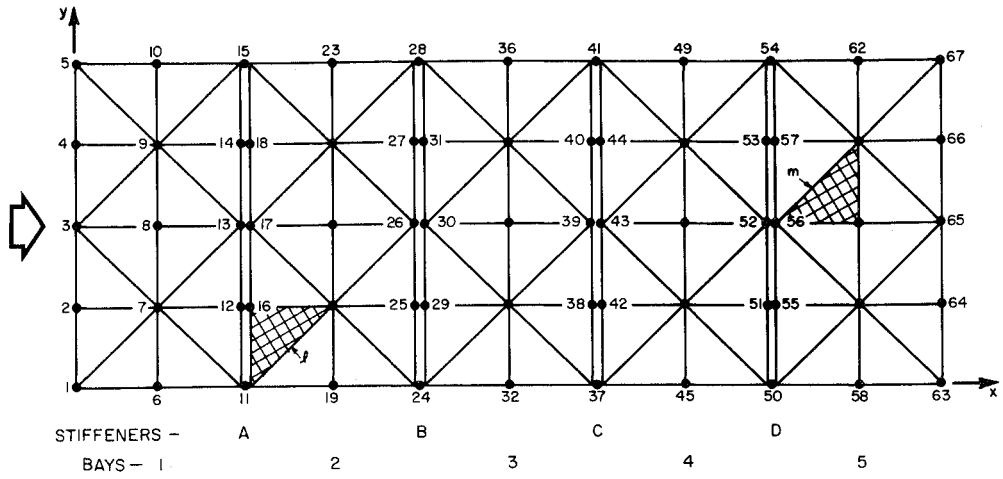

Fig. 8 Finite element representation for complete panel.

(x_1,y_1) and (x_2,y_2) are found from

$$\phi_{ww}(x_1,y_1;x_2,y_2;\omega) = \sum_{j,k=1}^{\infty}\sum f_j(x_1,y_1)f_k(x_2,y_2)H_j(\omega)H_k^*(\omega)I_{jk}(\omega) \quad (5)$$

where

$$H_j(\omega) = m_j^{-1}(\omega_j^2 - \omega^2 + 2i\zeta_j\omega\omega_j)^{-1} \quad (6)$$

is the usual admittance for the jth mode. Even though this analysis is easy in principle, the integrations involved in Eq. (4) have in the past been formidable except for the simplest problems with simple mode shapes. Now however, the difficulties can be overcome with the versatile finite element method.

Table 1 Comparison of predicted and measured vibration frequencies

Mode	Symmetry x	Symmetry y	Theory (Hz)	Experiment (Hz)
	1	1		
1	S	S	623.50	609
2	A	S	630.98	634
3	S	S	638.65	651
4	A	S	673.78	669
5	S	S	673.79	682
	1	2		
6	S	A	915.47	897
7	A	A	920.53	910
8	S	A	926.71	917
9	A	A	935.04	928
10	S	A	935.35	945
	1	1	Stringer bending	
11	A	S	1160.8	1175
12	S	S	1210.5	1245
13	A	S	1288.4	1330
14	S	S	1394.6	1429
	1	3		
15	S	S	1329.3	1324
16	S	S	1332.5	1333
17	A	S	1333.0	1345
18	S	S	1338.2	1350
19	A	S	1340.8	1375
	2	1		
20	A	S	1606.6	1604
21	S	S	1748.5	1674
22	A	S	1924.3	1982
23	S	S	2107.7	2185
24	A	S	2258.6	2353

Consistent Finite Element Approach

The analysis begins with the eigenvectors determined in Sec. 2. These are expanded and distributed according to the boundary, symmetry and constraint conditions over the gridwork for the full panel shown in Fig. 8. This yields 402 long eigenvectors each of which defines a mode shape over the whole panel in a piecewise finite element sense. That is, a mode shape distribution may be written formally as

$$f(x,y) = \sum_{l=1}^{80} w_l(x,y) \quad (7)$$

$w_l(x,y)$ is the displacement distribution over the lth element, which comes from the polynomial used in the element formulation and is uniquely determined once the degrees of freedom are specified at the element vertices. Following Ref. 18, this distribution may be written in terms of the element's local coordinates (ξ,η) as

$$w_l(x,y) = \{W\}_l^T[R]_l^T[T_2]_l^T\{F(\xi,\eta)\} \quad (8)$$

where $\{F(\xi,\eta)\}$ is the 20 long column vector of polynomial terms used in the finite element formulation.

The integrations involved in Eq. (4) are too complicated to carry out in closed form for the cross spectral density function of Eq. (3), and some approximation must be introduced. Considering the arbitrary general triangular elements l and m shown in Fig. 9, the cross spectral density distribution over each of these elements may be approximated by a linear func-

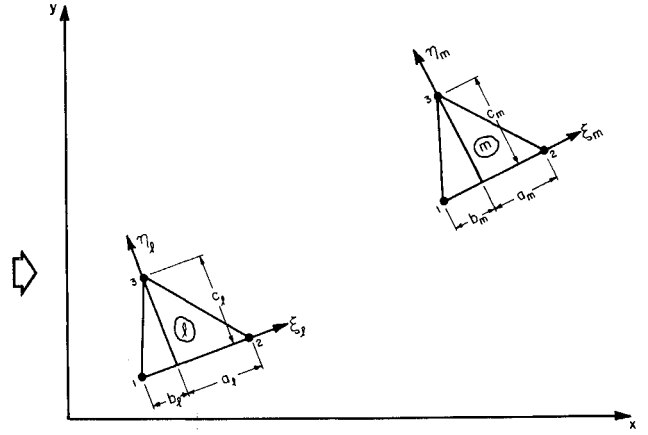

Fig. 9 General Triangular elements in propagating noise field.

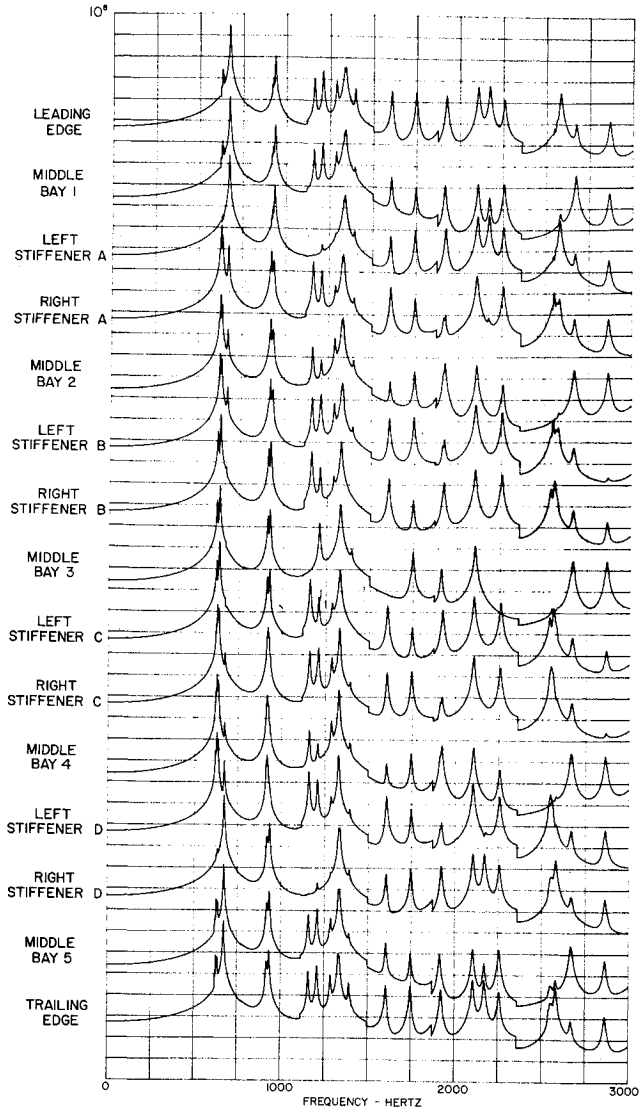

Fig. 10 σ_x stress spectra along panel quarterline.

tion of the local coordinates.‡ That is,

$$\phi_{pp} = e_1 + e_2\xi_l + e_3\eta_l + e_4\xi_m + e_5\eta_m + e_6\xi_l\xi_m + e_7\xi_l\eta_m + e_8\eta_l\xi_m + e_9\eta_l\eta_m \quad (9)$$

The nine arbitrary constants in this expression are determined by evaluating ϕ_{pp} nine times for nine combinations of the three vertices of each triangle. Thus

$$\begin{aligned}\phi_1 &= \phi_{pp}(x_{m1} - x_{l1}, y_{m1} - y_{l1}, \omega)\\ \phi_2 &= \phi_{pp}(x_{m1} - x_{l2}, y_{m1} - y_{l2}, \omega)\\ &\cdots\cdots\cdots\cdots\\ &\cdots\cdots\cdots\cdots\\ \phi_9 &= \phi_{pp}(x_{m3} - x_{l3}, y_{m3} - y_{l3}, \omega)\end{aligned} \quad (10)$$

where (x_{mr}, y_{mr}) are the global coordinates of the rth node on the mth element. Substituting into Eq. (9) for the nine combinations yields

$$[T_3]\{E\} = \{\Phi\} \quad (11)$$

‡ This is the next approximation to that introduced in Ref. 19, namely that the cross spectral density was constant over each triangular element.

where $[T_3]$ is

$$\begin{bmatrix} 1 & -b_l & 0 & -b_m & 0 & b_lb_m & 0 & 0 & 0 \\ 1 & a_l & 0 & -b_m & 0 & -a_lb_m & 0 & 0 & 0 \\ 1 & 0 & c_l & -b_m & 0 & 0 & 0 & -c_lb_m & 0 \\ 1 & -b_l & 0 & a_m & 0 & b_lb_m & 0 & 0 & 0 \\ 1 & a_l & 0 & a_m & 0 & -a_lb_m & 0 & 0 & 0 \\ 1 & 0 & c_l & a_m & 0 & 0 & 0 & c_la_m & 0 \\ 1 & -b_l & 0 & 0 & c_m & 0 & -b_lc_m & 0 & 0 \\ 1 & a_l & 0 & 0 & c_m & 0 & a_lc_m & 0 & 0 \\ 1 & 0 & c_l & 0 & c_m & 0 & 0 & 0 & c_lc_m \end{bmatrix} \quad (12)$$

Eq. (12) may be easily inverted either numerically or in closed form to yield the constants e_i as

$$\{E\} = [T_3^{-1}]\{\Phi\} \quad (13)$$

For the present application, this linear approximation should provide reasonable accuracy up to frequencies of 3000 Hz, where the characteristic element size is still less than half a wave length in the noise.

Now substituting Eqs. (7–9) into Eq. (4) with proper matrix considerations yields

$$I_{jk}(\omega) = \sum_{l,m=1}^{80}\sum \{W\}_{lj}{}^T[R]_l{}^T[T_2]_l{}^T \iint_{\Delta_l} \iint_{\Delta_m} \{F(\xi_l,\eta_l)\} \times (e_1 + - - + e_9\eta_l\eta_m)\{F(\xi_m,\eta_m)\}^T d\xi_l d\eta_l d\xi_m d\eta_m \times [T_2]_m[R]_m\{W\}_{mk} \quad (14)$$

where the extra j and k subscripts on $\{W\}$ refer to the j and k modes, respectively. Note that each of the full integrations of Eq. (4) has thus become a sum of eighty integrations over individual elements denoted by Δ_l and Δ_m as shown. Introducing the following notation for the integrals in Eq. (14)

$$\begin{aligned}\{P_0\}_l &= [R]_l{}^T[T_2]_l{}^T \iint_{\Delta_l} \{F(\xi,\eta)\}d\xi d\eta\\ \{P_1\}_l &= [R]_l{}^T[T_2]_l{}^T \iint_{\Delta_l} \xi\{F(\xi,\eta)\}d\xi d\eta\\ \{P_2\}_l &= [R]_l{}^T[T_2]_l{}^T \iint_{\Delta} \eta\{F(\xi,\eta)\}d\xi d\eta\end{aligned} \quad (15)$$

it is seen that $\{P_0\},\{P_1\},\{P_2\}$ are the 18 long consistent load vectors for loads uniform, linear in ξ, and linear in η, respectively, transformed to the (x,y) global coordinate system. Eq. (14) then reduces to

$$I_{jk}(\omega) = \{\psi\}_j{}^T[Q(\omega)]\{\psi\}_k \quad (16)$$

where

$$[Q(\omega)] = \sum_{l,m=1}^{80}\sum [e_1\{P_0\}_l\{P_0\}_m{}^T + e_2\{P_1\}_l\{P_0\}_m{}^T + e_3\{P_2\}_l\{P_0\}_m{}^T + \ldots + e_8\{P_2\}_l\{P_1\}_m{}^T + e_9\{P_2\}_l\{P_2\}_m{}^T] \quad (17)$$

Table 2 Modes included in spectral calculations

Mode groups →		1	2	3	4	5	6	7	8	9	10
Frequency ranges	Modes / Center freqs.	1 to 5	6 to 10	11 to 14	15 to 19	20 to 24	25 to 29	30 to 34	35 to 39	40 to 44	45 to 49
0–777	650	×	×	×	×						
777–1118	925	×	×	×	×						
1118–1500	1300	×	×	×	×	×					
1500–1873	1700			×	×	×	×	×			
1873–2360	2100					×	×	×	×	×	
2360–3000	2600					×		×	×	×	×

and $\{\psi\}_j$ is the 402 long jth eigenvector. The load vector products $\{P_0\}_l\{P_0\}_m{}^T$, etc. are dyadic products and represent 18×18 matrices for each combination of l and m. Hence, Eq. (17) requires a double summation over all 80 elements, whereas the usual structural matrices require only one. The foregoing calculations must be carried out for each value of frequency ω, since the e_i depend on frequency. Note that $[Q]$ is complex, although Hermitean. Once the $I_{jk}(\omega)$ are known, the power spectral densities for displacements and stresses are easily calculated from Eq. (5).

Practical Calculations

In the present work, the calculations of $[Q]$ from Eq. (17) were carried out for only a few frequencies, namely at 650, 925, 1300, 1700, 2100, and 2600 Hz. These frequencies correspond to the centers of the main mode groups predicted in Sec. 2. The $I_{jk}(\omega)$ obtained for these frequencies were then held constant over these groups. The modes included in the spectral calculations in the vicinity of these center frequencies are indicated by the crosses in Table 2. The cross terms *within* each included mode group were retained in these calculations, but all other cross terms were neglected on the basis of the larger frequency separations. The frequency step sizes were made small in the vicinity of peaks and wider away from them. Finally, the spectra were numerically integrated over frequency using Simpson's rule to obtain mean square predictions for both displacements and stresses. All calculations were limited to the finite element nodes.

All the resulting spectra are presented together in Ref. 20 to facilitate comparisons over the panel. Fig. 10 shows some typical stress spectra. The ordinate is a logarithmic scale

Table 3 Predicted root mean square values

	Complete Calculations				Diagonal Terms Only,
	Band 1 0–777 Hz	Band 1–2 0–1118 Hz	Band 1–3 0–1500 Hz	Band 1–6 0–3000 Hz	Band 1–6 0–3000 Hz
Deflections			$10^2\, w_{\text{rms}}/p_o$		
Center-line—Middle of Bays					
Bay 1	6.160	6.168	6.216	6.216	6.280
Bay 2	5.505	5.511	5.581	5.581	6.628
Bay 3	5.712	5.718	5.802	5.802	5.756
Bay 4	7.394	7.398	7.486	7.487	6.628
Bay 5	6.270	6.278	6.356	6.356	6.280
Quarter-line—Middle of Bays					
Bay 1	3.652	3.725	3.793	3.794	3.855
Bay 2	3.243	3.330	3.419	3.420	4.091
Bay 3	3.354	3.450	3.565	3.565	3.519
Bay 4	4.360	4.495	4.611	4.611	4.091
Bay 5	3.722	3.828	3.940	3.940	3.855
Stresses in x-Direction			$10^{-4}\sigma_{x\text{rms}}/p_o$		
Center-line					
Leading Edge	2.915	2.919	2.975	2.990	3.023
Middle Bay 1	1.756	1.758	1.800	1.801	1.824
Stiffener A Left	2.571	2.574	2.608	2.622	2.633
Right	2.152	2.155	2.234	2.249	2.633
Middle Bay 2	1.433	1.435	1.498	1.500	1.785
Stiffener B Left	2.199	2.202	2.276	2.289	2.713
Right	2.278	2.280	2.367	2.378	2.381
Middle Bay 3	1.481	1.483	1.559	1.562	1.539
Stiffener C Left	2.336	2.338	2.424	2.435	2.381
Right	2.950	2.952	3.039	3.050	2.712
Middle Bay 4	1.929	1.930	2.005	2.007	1.785
Stiffener D Left	2.837	2.839	2.930	2.943	2.633
Right	2.580	2.583	2.641	2.655	2.633
Middle Bay 5	1.790	1.792	1.856	1.857	1.824
Trailing Edge	2.967	2.971	3.049	3.064	3.023

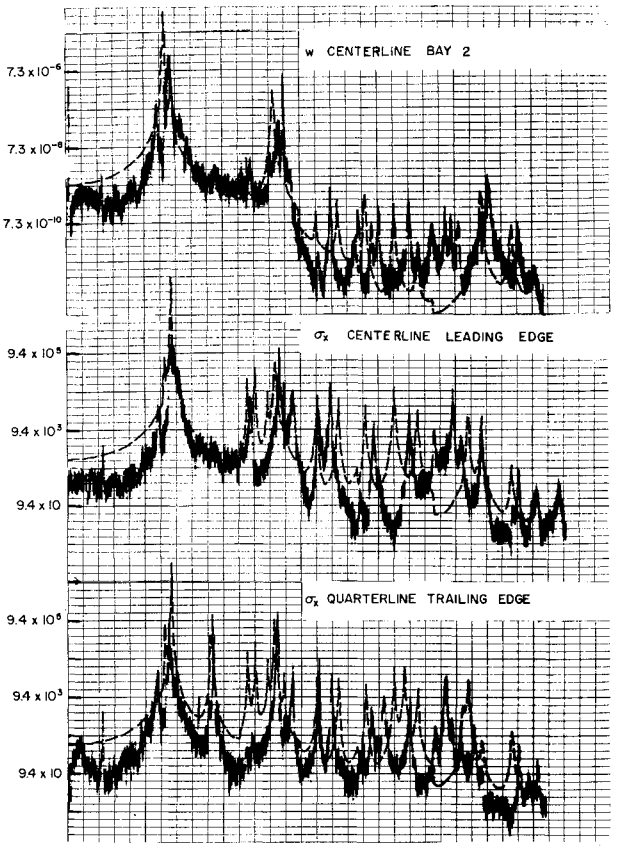

Fig. 11 Theoretical and experimental spectra.

with each grid line representing a factor of 10, and each curve is dropped 3 grid lines below the one above. Many individual modal peaks may be recognized, although those in the narrower bands tend to be merged together into one wide peak.

Some typical rms predictions are tabulated in Table 3. The table shows results from terminating the integrations at various frequencies and therefore reveals from where the major contributions are derived. It is clear that the first band predominates in all cases, particularly for the centerline results. The quarterline quantities appear to receive an appreciable contribution from band 3, probably mainly from modes 15–19 which have three half waves in the y direction. As to be expected, the rms stresses receive more from the higher modes than the rms displacements do. It appears that band 1 provides no less than 80% of the final rms value for all quantities and as much as 95% for some of the centerline deflections.

A further calculation was carried out in which all nondiagonal terms in Eq. (5) were neglected. The resulting spectra were plotted, but were very little different from those obtained from the more complete calculations. However, the rms results obtained from integrating these spectra did change somewhat and are given in the last column of Table 3. The first noticeable effect is that of symmetry down the panel. That is, the prediction for bay 4 is the same as for bay 2, etc., when only diagonal terms are retained. Hence, it appears that the results for bays 2 and 4 are changed the most, by as much as 20%. The results for bays 1, 3, and 5 apparently are altered very little by the off diagonal terms.

Finally, it is noted that the preliminary results of Ref. 19 using the constant cross spectra per finite element approximation were completely verified by the present calculations. That is, none of the predictions were changed by more than a few percent. In retrospect, this fact appears logical in that the most significant part of the predictions occurs in band 1

Table 4 Comparison of experimental and predicted root mean square values

	Experimental	Theory	Ratio
Deflections		$10^2\ w_{rms}/p_o$	
Centerline-line—Middle of Bays			
Bay 1	4.2	6.216	0.69
Bay 2	3.7	5.581	0.66
Bay 3	3.1	5.802	0.53
Bay 4	4.0	7.487	0.53
Bay 5	3.4	6.356	0.53
Quarter-line—Middle of Bays			
Bay 1	2.6	3.794	0.69
Bay 2	2.8	3.420	0.82
Bay 3	2.1	3.565	0.59
Bay 4	2.8	4.611	0.61
Bay 5	2.7	3.940	0.69
Stresses in x-Direction		$10^{-4}\ \sigma_{xrms}/p_o$	
Center-line			
Leading Edge	1.6	2.990	0.54
Stiffener A Left	1.2	2.622	0.46
Right	1.2	2.249	0.53
Stiffener B Left	1.2	2.289	0.52
Right	1.1	2.378	0.46
Stiffener C Left	0.9	2.435	0.37
Right	1.1	3.050	0.36
Stiffener D Left	0.9	2.943	0.31
Right	1.1	2.655	0.41
Trailing Edge	1.3	3.064	0.42
Quarter-Line			
Leading Edge	0.9	1.818	0.50
Stiffener A Left	0.7	1.605	0.44
Right	0.6	1.415	0.42
Stiffener B Left	0.7	1.436	0.49
Right	0.6	1.508	0.40
Trailing Edge	0.9	1.905	0.47
Stresses in y-Direction		$10^{-4}\ \sigma_{yrms}/p_o$	
Middle of Bay 1			
Bottom	0.7	1.339	0.52
Middle of Bay 5			
Bottom	0.8	1.483	0.54

from 600 to 700 Hz, and for this frequency range, the constant cross spectra per element approximation is quite satisfactory.

Panel Response Measurements

The random response tests were carried out with the panel inserted in the rigid baffle as shown schematically in Fig. 5. Displacement measurements were made with noncontacting inductance probes of $\frac{1}{4}$ in. diam. Stress measurements were made with single foil strain gauges $\frac{1}{16}$ in. wide by $\frac{3}{16}$ in. long adhered with Eastman 9–10 cement to the underside of the panel. All these gauges had their centers positioned about $\frac{1}{8}$ in. away from the panel boundaries and/or stiffeners where maximum stresses are to be expected.

Root mean square measurements of all displacement and strain signals were made with a Bruel and Kjaer true rms meter and spectral analyses of the same signals were made on-line with the aforementioned G.R. wave analyzer. The spectra were all taken with a bandwidth of 3 Hz, pen writing speed of 1 in./sec and traverse speed of 62.5 Hz/min. Some typical spectra are presented in Fig. 11 along with the corresponding theoretical predictions shown dashed. Note that the experimental spectra are one sided, and hence, have been lowered by a factor of 2 to compare with the double-sided predictions. The measured and predicted rms results are presented in Table 4 along with ratios of the former to the latter. It appears that the predictions over the first band from 600 to 700 Hz are higher than the experimental measurements. The differences here are larger for stresses than for displacements. Some similar but smaller differences may be observed for the 900 Hz band as well. On the other hand, the experimental and predicted spectra levels around 1300 Hz compare quite well. Above 1300 Hz, the displacement spectral fall off much more rapidly than the stress spectra.

It is seen that in general most of the detailed individual peaks are lost within the bands of modes, especially in the experimental results. There are some exceptions of course, notably with respect to modes which have nodal lines parallel to the stiffeners. Some of these other modes are readily identifiable by their individual peaks, for example modes 11–14, 20–24 and 45–49. These modes are not closely spaced in frequency, but rather are far apart and hence may respond on an individual basis. It is also interesting to note that some of these modal responses compare very well with the predictions. This may be associated with the fact that their experimental mode shapes also compared well with the predictions.

Some of the discrepancy between theory and experiment around 600 Hz is due to the overpredictions of the noise spectra model. Earlier, it was noted that this model could have been too high by a factor of 2 in this range. Other discrepancies are due to differences in experimental and predicted mode shapes. The I_{jk} terms of Eq. (4) are especially sensitive to mode shape. Finally, there is still considerable doubt about what the proper damping is.

From Table 4, it is seen that the measured rms displacements ranged from 53% to 82% of the predictions and the rms stresses ranged from 31% to 53% of their predictions. Some of the larger discrepancy in stresses is due to the finite length of the strain gauges and their positions away from the stiffeners and boundaries. The predictions are for points right at those boundaries and there is a rapid decay of bending moments away from them. Again it is noted that most of the rms predictions come from band 1, and if this band is over predicted so also will the rms values be. This suggests that it would be better to use an actual experimental noise spectra as input for this first important band. However, in light of the unknowns with respect to mode shapes and damping, this alone would not seem justified, although there is no doubt that such a procedure would improve the comparisons in the present work. However, whether or not this would generally be true is still largely unknown. The writers preferred to leave the comparisons as they stand, i.e., on the basis of a completely theoretical prediction including input spectra model, until such time as more work is done on mode shapes and damping.

Conclusions

The free vibrations and random response to jet noise of an integrally stiffened five bay panel have been studied both theoretically and experimentally. A finite element approach was used to represent the panel for both parts of the study, and the predictions were verified by measurements on a model panel integrally machined from solid Aluminum stock.

The measured and predicted frequencies compared extremely well for the first fifty modes with differences between the two growing for some of the higher modes above fifty. The comparison between mode shapes was not nearly so good. The best comparisons were obtained for modes with nodal lines parallel to the stiffeners and the poorest, for those with nodal lines perpendicular to them. These observed effects appeared to be due to slight imperfections in the panel, and this suggests that the latter type of modes is more sensitive to such imperfections than the former.

The predicted displacement and stress spectra for the panel exhibited relatively wide over-all peaks for each band of modes. Most of the individual peaks within each band were lost, particularly for the narrower bands. The main exceptions to this were those modes with nodal lines parallel to the

stiffeners. These modes being relatively wider separated exhibited the more customary individual peaks. These predictions for these latter modes were verified by the measured ones, at least in a qualitative sense. The predictions over band 1 (600–700 Hz) were generally too high partly because the model input spectra was too high in this region. The predicted and measured spectra tended to agree better at the higher frequencies. The measured rms displacements were about 60% of the predictions, while the stresses were about 45%.

References

[1] Trapp, W. J. and Forney, D. M., Jr., eds., U.S. Air Force, WADC TR 59-676, University of Minnesota Conference on Acoustical Fatique, 1961, Wright Air Development Center, Ohio.

[2] Trapp, W. J. and Forney, D. M., Jr., eds., "Acoustical Fatigue in Aerospace Structures," *Proceedings of the Second International Conference, Dayton, Ohio, April 29–May 1, 1964*, Syracuse University Press, 1965.

[3] Richards, E. J. and Mead, D. J., eds., *Noise and Acoustic Fatigue in Aeronautics*, Wiley, London, England, 1968.

[4] Lin, Y. K. and Donaldson, B. K., "A Brief Survey of Transfer Matrix Techniques with Special Reference to the Analysis of Aircraft Panels," *Journal of Sound and Vibrations*, Vol. 10, No. 1, Jan. 1969, pp. 103–143.

[5] Mercer, C. A. and Seavey, C., "Prediction of Natural Frequencies and Normal Modes of Skin-Stringer Panel Rows," *Journal of Sound and Vibrations*, Vol. 6, No. 1, Jan. 1967, pp. 149–162.

[6] Clarkson, B. L. and Cicci, F., "Methods of Reducing the Response of Integrally Stiffened Structures to Random Pressures," Paper 69-Vibr-26, 1969, American Society of Mechanical Engineers.

[7] Lindberg, G. M. and Olson, M. D., "Vibration Modes and Random Response of a Multi-Bay Panel System Using Finite Elements," Aeronautical Rept. LR-492, 1967, National Research Council of Canada.

[8] Rudder, F. F., Jr., "Dynamic Analysis of a Stiffened Flat Panel Array," Research Rept. ER-9714, 1969, Lockheed-Georgia Co.

[9] Jacobs, L. D., Lagerquist, D. R., and Gloyna, F. L., "Response of Complex Structures to Turbulent Boundary Layers," *Journal of Aircraft*, Vol. 7, No. 3, May-June 1970, pp. 210–219.

[10] Powell, A., "On Fatigue Failure of Structures Due to Vibrations Excited by Random Pressure Fields," *Journal of the Acoustic Society of America*, Vol. 30, 1958, pp. 1130–1135.

[11] Lin, Y. K., *Probabilistic Theory of Structural Dynamics*, McGraw-Hill, New York, 1967.

[12] Maestrello, L., Gedge, M. R., and Reddaway, A. R. F., "The Response of a Simple Panel to the Pseudo-Sound Yield of a Jet," *Proceedings of Air Force Office of Scientific Research—University of Toronto Institute of Aerospace Studies Symposium on Aerodynamic Noise, May 20–21, 1968*, University of Toronto Press, 1968, pp. 189–208; also Doc. D1-82-0652, 1967, Boeing Scientific Research Lab.

[13] Wilby, J. F., "The Response of Simple Panels to Turbulent Boundary Layer Excitation," TR AFFDL-TR-67-70, 1967, U.S. Air Force Flight Dynamics Lab.

[14] Blackman, D. R., Clark, D. M., McNulty, G. J., and Wilby, J. F., "Boundary Layer Pressure Fluctuations and Structural Response," TR AFFDL-TR-67-97, 1967, U.S. Air Force Flight Dynamics Lab.

[15] Newsom, C. D., Fuller, J. R., and Sherrer, R. E., "A Finite Element Approach for the Analysis of Randomly Excited Complex Elastic Structures," *AIAA/ASME 8th Structures, Structural Dynamics and Materials Conference*, AIAA, New York, 1967.

[16] Ballentine, J. R., Rudder, F. F., Jr., Mathis, J. T., and Plumblee, H. E., Jr., "Refinement of Sonic Fatigue Structural Design Criteria," TR AFFDL-TR-67-156, 1968, U.S. Air Force Flight Dynamics Lab.

[17] Cowper, G. R., Kosko, E., Lindberg, G. M., and Olson, M. D., "A High Precision Triangular Plate Bending Element," Aeronautical Rept. LR-514, 1968, National Research Council of Canada.

[18] Cowper, G. R., Kosko, E., Lindberg, G. M., and Olson, M. D., "Static and Dynamic Applications of a High Precision Triangular Plate Bending Element," *AIAA Journal*, Vol. 7, No. 10, Oct. 1969, pp. 1957–1965.

[19] Olson, M. D. and Lindberg, G. M., "Free Vibrations and Random Response of an Integrally Stiffened Panel," *Proceedings of Conference on Current Developments in Sonic Fatigue*, Univ. of Southampton, July 6–9, 1970, R. E. Gordon and Co., London, England.

[20] Olson, M. D. and Lindberg, G. M., "Free Vibrations and Random Response of an Integrally Stiffened Panel," Aeronautical Rept. LR-544, 1970, National Research Council of Canada.